corrosion and materials degradation

MDPI

Article

Performance of Phenolic-Epoxy Coatings after Exposure to High Temperatures †

Saleh Ahmed [1,*], Katerina Lepkova [1], Xiao Sun [2], William D. A. Rickard [2] and Thunyaluk Pojtanabuntoeng [1]

[1] Curtin Corrosion Centre, Western Australia School of Mines, Mineral, Energy and Chemical Engineering, Curtin University, Technology Park, Bentley, WA 6102, Australia
[2] John de Laeter Centre, Curtin University, Bentley, WA 6102, Australia
* Correspondence: saleh1399@gmail.com
† This paper is a part of the PhD Thesis of Investigating the Corrosion Characteristics of Carbon Steel and the Efficacy of Phenolic-Epoxy Coatings in Enclosed Environments, presented at the Curtin University of Perth, Perth, WA 6102, Australia

Abstract: Phenolic-epoxy coatings, which are designed to protect substrates from thermal damage, are widely applied in many fields. There remains an inadequate understanding of how such coatings change during their service life after exposure to various temperature conditions. To further elucidate this issue, this case study investigated the effects of high temperatures on carbon steel panels coated with phenolic epoxy and exposed to different heating conditions. A general trend of decreasing barrier performance was observed after exposure to 150 °C for 3 d, as evidenced by the appearance of cracks on the panel surfaces. In contrast, the coating performance improved after exposure to isothermal conditions (120 °C) or thermal cycling from room temperature to 120 °C, as indicated by the increased low-frequency impedance modulus values of the coating. This unexpected improvement was further examined by characterising the coatings using transform infrared spectroscopy (FTIR), thermogravimetric analysis (TGA), differential scanning calorimetry (DSC), pull-off adhesion tests, and time-of-flight secondary ion mass spectrometry (ToF-SIMS). The maximum pull-off adhesion force (24.9 ± 3.6 MPa) was measured after thermal cycling for 40 d.

Keywords: carbon steel; EIS; ToF-SIMS; phenolic epoxy; pull-off adhesion

Citation: Ahmed, S.; Lepkova, K.; Sun, X.; Rickard, W.D.A.; Pojtanabuntoeng, T. Performance of Phenolic-Epoxy Coatings after Exposure to High Temperatures. *Corros. Mater. Degrad.* **2024**, *5*, 73–91. https://doi.org/10.3390/cmd5010004

Academic Editors: Wolfram Fürbeth and Marjorie Olivier

Received: 26 July 2023
Revised: 19 February 2024
Accepted: 26 February 2024
Published: 29 February 2024

1. Introduction

Corrosion protection of metallic substrates is a traditional application of organic coatings, which remains one of the most cost-effective means of providing practical corrosion protection. Controlling corrosion by applying coatings is very important, especially for structures that are subjected to corrosive environments during use. If failure of the protective coating occurs, the functionality of the coated structure can be threatened. The main goal of corrosion-protection coatings is to provide long-term protection to increase the practical service life of the substrate [1]. In certain applications, the coating must be sufficiently flexible to withstand deformation due to thermal expansion/contraction. Cracks must not occur during heating after the coating is cured, as this indicates the degradation of the polymer coating, which may result in eventual adhesive failure [2].

Epoxy coatings are two-component systems consisting of an epoxy compound and a hardener, which react to form a cured network [3]. Phenolic epoxy coatings are an effective and inexpensive method for providing protection against thermal damage and corrosion under insulation (CUI) [4]. To prevent corrosion on metallic structures, epoxy resins (ER), which are polymeric materials, are widely used in coating preparations [5–7]. Through their adsorption at the interface between metallic surfaces and the environment, the polymeric ERs physically form barriers which separate the metallic materials from the unfriendly environment and try to slow down the metallic corrosion rate [8–10]. The polymer cross-links to form a network during curing, resulting in a coating with high resistance to

heat and the diffusion of corrosive substances, which is considered an important factor governing the physical properties of the cured resin and corrosion resistance, particularly for amine- or anhydride-cured ERs [11]. However, there is no clear consensus on the effect of cross-linking on the coating performance, partly because the methods for changing the cross-linking density introduce problems, such as changes in the chemical structure of epoxy resin or hardener when exposed to high temperatures [12]. This can damage the polymer network by chemical bond scission (chain scission), which creates small molecular fragments [2].

The aim of this case study was to evaluate the behaviour of a phenolic epoxy under thermal exposure. Many methods were used to characterise the chemical and physical changes in the phenolic epoxy, such as pull-off adhesion, EIS, TGA, DSC, FTIR, and ToF-SIMS. These methods provided information about the cross-linked structures after the degradation of the epoxy coatings and the thermal stability of the coatings under different conditions.

2. Experimental

2.1. Materials

Carbon steel plates (AS36/Grade 250) with a nominal composition of 0.04 C, 0.2 Si, 5.5 M, 0.005 P, 0.003 S, 0.03 Al, 0.22 Mo, 0.30 Ni, 0.39 Cr, and balance of Fe (wt%) (Bluescope steel, New South Wells, Australia), and dimensions of 170 mm × 50 mm × 6 mm were used as substrates. The surface preparation grade of test panels immediately before coating application complied with ISO 8501-1: 2007, Sa 3. The steel plates were coated with a commercial amine-cured phenolic-epoxy coating (Dulux coating company, Clayton South, VIC, Australia). The chemical composition of the coating is shown in Table 1. The supplier applied one layer of the epoxy coating to the carbon steel substrates using an airless spray gun. The coating thickness was measured using a digital gauge (PosiTector 6000) with the appropriate gauge and calibration standards (MP 2527) (AT advance tools, Adelaide, Australia). Measurements were performed at a minimum of five points on the sample surface. The maximum operating temperature of the coating is 120 °C (dry heat).

Table 1. Composition of the phenolic epoxy coating.

Phenolic Epoxy	Proportion
Bisphenol-A epoxy resin	10–30%
Benzyl alcohol	1–10%
Bisphenol-F epoxy resin	1–10%
Methylisobutyl ketone	1–10%
Xylene	1–10%
Amine hardener	Proportion
Isophorone diamine	>60%

2.2. Exposure Conditions

The coated panels were divided into two groups (six samples each) and exposed to dry heat in an oven (Binder GmbH, FDL 115, Tuttlingen, Germany). The isothermal group was dried at a constant temperature (120 °C), while for the cyclic group was subjected to thermal cycling (22 to 120 °C) following ISO 19277:2018 (dry thermal cycling) [13]. The thermal cycling process is illustrated in Figure 1.

The samples for thermal cycling were removed from the oven, cooled at room temperature for 4 h, and then placed into the oven again at 120 °C for 20 h (temperature rise rate was 10 °C/min). The isothermal and cycled samples were taken out of the furnace for examination after 20, 40, and 60 d. Additionally, one coated panel was exposed to 150 °C under isothermal conditions to accelerate the thermal degradation.

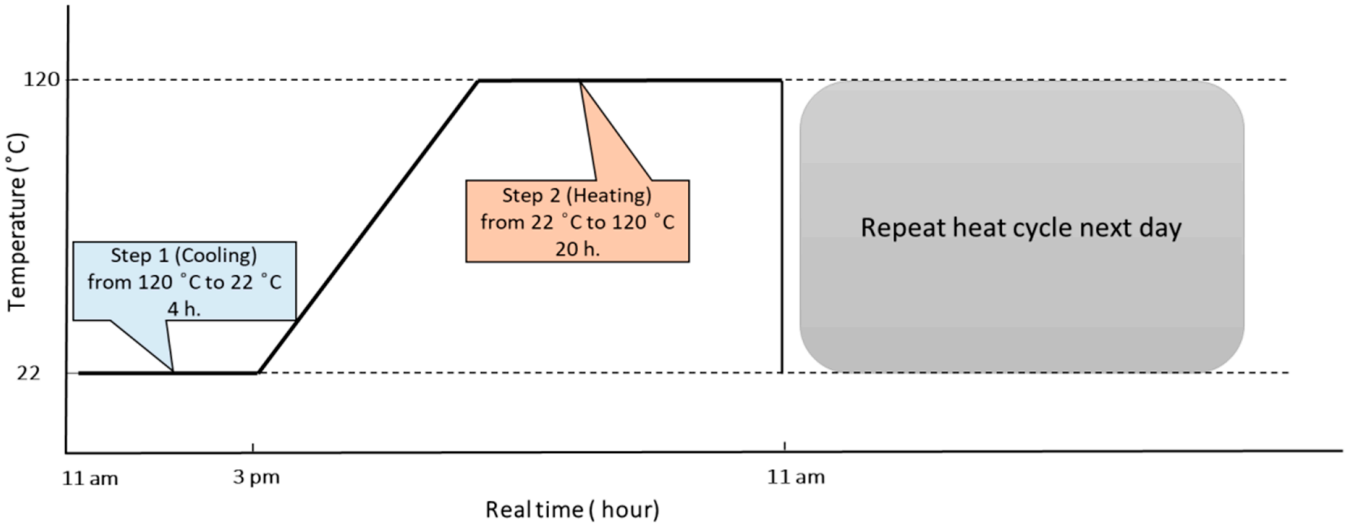

Figure 1. Dry thermal cycling profile (temperature vs. time).

2.3. Characterisation Techniques

2.3.1. Pull-Off Adhesion Strength

During adhesion-strength testing, the force required to pull a specified test diameter of a coating away from its substrate using a hydraulic pump is measured. Adhesion tests were conducted using an automatic adhesion tester (PosiTest® AT-A) (DeFelsko company, Ogdensburg, NY, USA) following ASTM D4541-02 [8,14]. The aluminium dolly was 14 mm in size. All dollies and the coating surface were abraded with 1200 grit SiC paper to enhance the mechanical anchoring with the adhesive. The dollies were cleaned with acetone to remove any contamination before they were affixed to the coating. The adhesion tests were performed 24 h after the dollies were affixed on the coated panels with epoxy adhesive (Resinlab EP11 HT) (REsilab adhesive company, New South Wales, Australia). The measurements were conducted in triplicate. Before attaching the dolly to the coating surface, the coating around the dolly was cut using a hole saw and removed. Equation (1) was used to calculate the percentage change in the adhesion strength of the coating, which compares the strengths before (pre-exposure) and after (post-exposure) the sample was exposed to dry heating.

$$\text{Adhesion strength change } (\%) = \frac{\text{post exposure}^{*} - \text{pre exposure}}{\text{post exposure}} \times 100 \quad (1)$$

* The pre-exposure adhesion strength was 11.6 ± 1.1 MPa.

2.3.2. Electrochemical Impedance Spectroscopy (EIS)

The performance of the coating before and after thermal exposure was evaluated using EIS. A glass tube with an exposed area of 14.6 cm^2 and 8 cm height was placed on the coated panel and tightly sealed with a mechanical clamp, as shown in Figure 2. The electrolyte was 3.5 wt% NaCl solution at 24 ± 1 °C and the total volume of electrolyte in the glass cell was 100 mL. A conventional three-electrode cell was used, consisting of an ionode probe filled with 3 M of KCl electrolyte as a reference electrode (with its tip placed 1–3 mm from the coating surface), a platinum mesh as a counter electrode, and the coated carbon steel as the working electrode. EIS measurements were conducted using a Gamry potentionstat (Interface 1010E^{TM}) (Scientific solution company, South Australia, Australia) at the OCP. A 20 mV (r.m.s) sinusoidal perturbation was applied in the frequency range of 100 KHz to 10 mHz, and six points per decade were measured. The EIS curves were analysed using Gamry Echem Analyst^{TM} software, version 7.8.

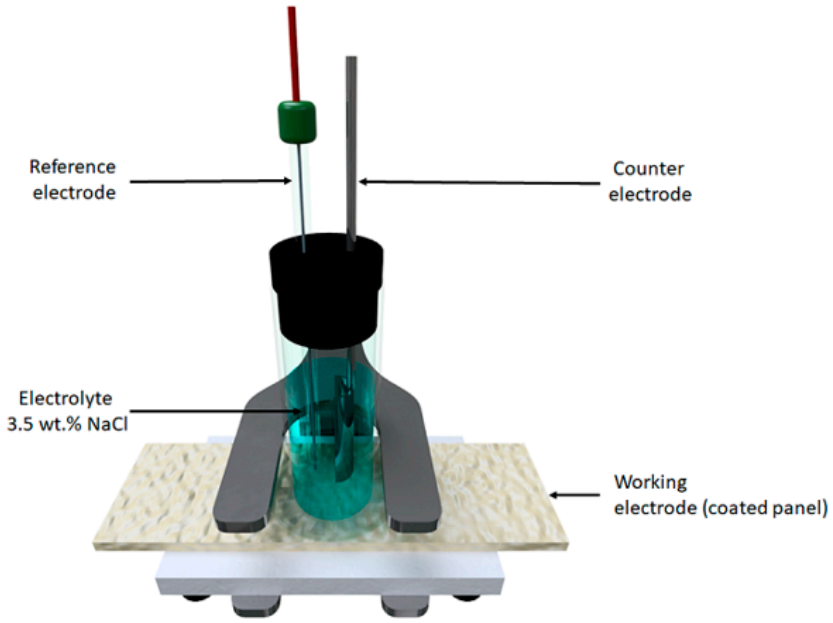

Figure 2. Schematic of the electrochemical cell used for testing the epoxy-coated metal sheets.

2.3.3. Thermal Analysis

A Mettler Toledo AG (Nänikon, Switzerland) system was used for both TGA and DSC. The measurements were conducted in the temperature range of 35–800 °C at the heating rate of 10 °C min^{-1} under an air flow (0.01 L min^{-1}). First, 5 mg samples scraped from the top layer of the coating surface were placed in a 40 µL platinum open pan. For TGA analysis, the sample weight as a function of temperature was measured. At the end of each run, the experimental data were used to plot the percentage of undegraded sample $(1 - D)$% as a function of temperature, where $D = (W_0 - W)/W_0$; W_0 and W are the masses of sample at the starting point and during scanning. The experiments were performed in duplicate to obtain weight loss data. The initial weight loss of the pre-exposed sample was related to water loss [15]. For DSC analysis, the heat flow of the samples was measured to evaluate the enthalpy and temperature of the observed phase transitions.

2.3.4. FTIR

FTIR was used to determine the chemical changes in the polymer chains and the behaviours of all bands that are generated in hydrocarbon chains as a result of thermal exposure. A Nicolet iS50 (ThermoFisher Scientfic, Waltham, MA, USA) was used to obtain the FTIR spectra, which is fitted with a dedicated single-bounce diamond ATR purged with dry nitrogen. Specimens were obtained by scraping several milligrams of material from the surface of the coating, which was then finely ground in an agate mortar. All samples were measured using 64-scan data accumulated over the range of 500–4000 cm^{-1} at a spectral resolution of 4 cm^{-1}.

2.3.5. ToF-SIMS

ToF-SIMS analyses were performed using an IONTOF M6 ToF-SIMS system operated with a Bi_3^+ primary ion source (30 keV) and an electron flood source for charge compensation. The pulsed primary ion beam current was 1.1 pA and the primary ion dose density was below the static SIMS limit of 10^{13} ions cm^{-2}. Positive ion mass spectra were acquired from 100 µm × 100 µm areas with a cycle time of 100 µs. The spectroscopy analytical mode was used, resulting in a mass resolution above 7500 at m/z = 29. SurfaceLab software (IONTOF Gmbh, Münster, Germany; version 7.2) with integrated multivariate statistical analysis was used to analyse the data. Principle component analysis was used to identify variations between spectra obtained from different samples.

Three coated panels were subjected to ToF-SIMS analysis, namely, a fresh sample used as a control, the sample exposed to 150 °C, and a selected sample after thermal exposure to cycling at 22 to 120 °C. Cross-sectional samples were prepared using a sandwich method (Figure 3) to minimise edge effects, which are deleterious for ToF-SIMS. The surface was prepared for analysis by wet grinding using SiC paper up to 1200 grit and then rinsing with deionised water and ethanol, followed by air drying.

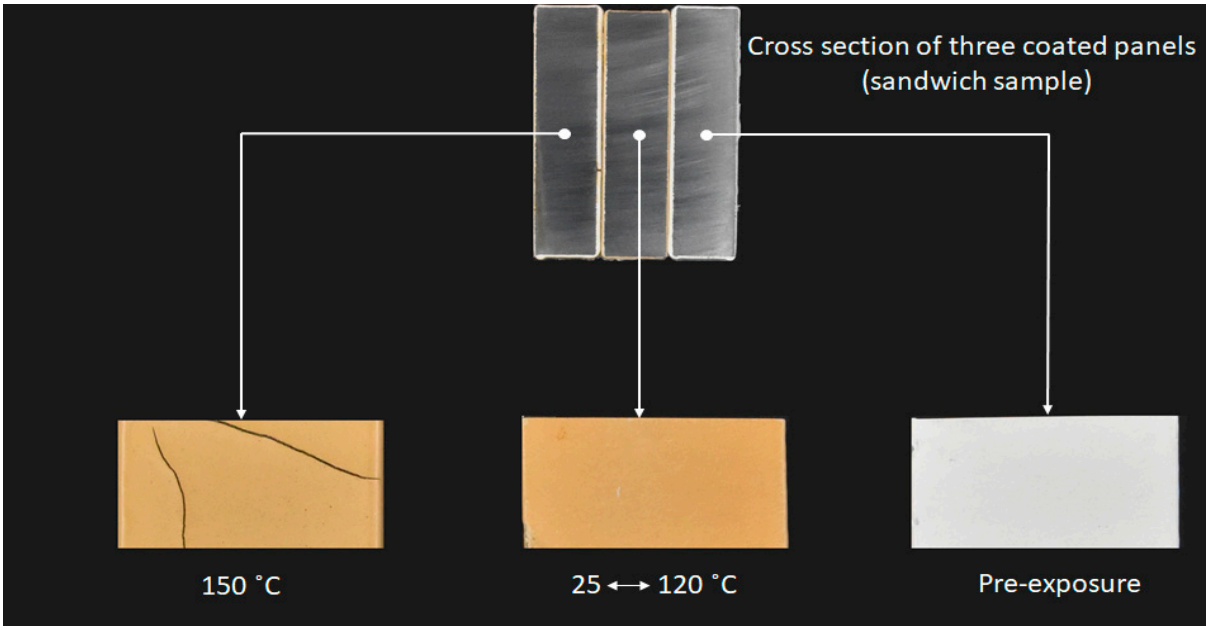

Figure 3. Arrangement of the three coated panels used for ToF-SIMS measurements.

3. Results and Discussion

3.1. Pull-Off Adhesion Strength

The pull-off strength measurements were conducted on the samples before and after 20, 40, and 60 days of exposure to isothermal or cyclic conditions (maximum temperature of 120 °C). Table 2 presents the adhesion strengths of the epoxy coatings as a function of time and dry heating condition. All tests were performed on duplicate coating panels with three measurements on each panel. As the exposure time increased from 0 to 60 d, the adhesion strength of all specimens increased. The highest value was ~24.9 MPa for the sample cycled for 40 d, corresponding to an increase of 53.4% compared to the initial condition. Moreover, the adhesion strength of the isothermal specimen after 40 d was high (20.2 MPa) with an increase of 42.6%. Furthermore, phenolic epoxy showed similar adhesion strengths (13.1–14.9 MPa) for all other exposure conditions and times. These results confirm that the adhesion properties of the organic coatings on the substrate improved for all samples after dry heat exposure. A previous study reported that the pull-off strength between the coating and metal substrate increases as the coating thickness decreases [16]. To confirm this, the coating thickness around the dolly was measured using a digital PosiTector 6000 (DeFelsko company, Ogdensburg, NY, USA), which indicated that the distance from the dolly to the edge of the coated panel was 16.0 ± 1 mm. Figure 4 compares the pull-off strength with the coating thickness around the dolly for all coated panels. The thickness varied between 163 and 320 µm. No obvious correlation between the coating thickness and pull-off strength was observed for the various samples, and most of the data points were under the fit line.

The area fractions of certain failure modes (cohesion, adhesion, and glue) of the detached adhesive surfaces after pull-off tests were calculated using ImageJ software, version 1.52t [17]. Cohesion is defined as the internal strength of an adhesive resulting from the various interactions within the adhesive (single material), while adhesion refers to the bonding between the coating and metal substrate (two materials). Furthermore, a mixed failure

mode describes the case when failure of cohesion and adhesion occurs simultaneously. In this case, the ratio between adhesive and cohesive areas can be determined. Additionally, failure can also occur in the adherent (i.e., the glue between the coating and dolly in these tests) if the adhesive is stronger than the adherent and the adhesive remains intact after test. Figure 5 shows the area fractions of the three failure modes (glue, cohesion, and adhesion) expressed as percentages. For the control sample (pre-exposure), adhesive failure is dominant. However, after thermal exposure, loss of cohesion is the major failure mode. As the pull-off adhesion tests measure the weakest bond among the coating/steel, coating, and coating/dolly, the results indicated that the bond strength between the coating/substrate increased after thermal exposure.

Table 2. Pull-off adhesion strengths for all tested samples.

Duration (Days)	Adhesion Force (MPa) at Constant Temperature	Adhesion Increase (%)	Average Thickness (µm)	Adhesion Force (MPa) at Cycling Temperature	Adhesion Increase (%)	Average Thickness (µm)
20	13.7 ± 0.75	15.3	265 ± 73	14.3 ± 1.61	18.9	215 ± 40.87
40	20.2 ± 2.9	42.6	210 ± 54	24.9 ± 3.6	53.4	195 ± 73.08
60	14.2 ± 2.4	18.3	220 ± 20.82	13.1 ± 2.2	11.5	168 ± 13.65

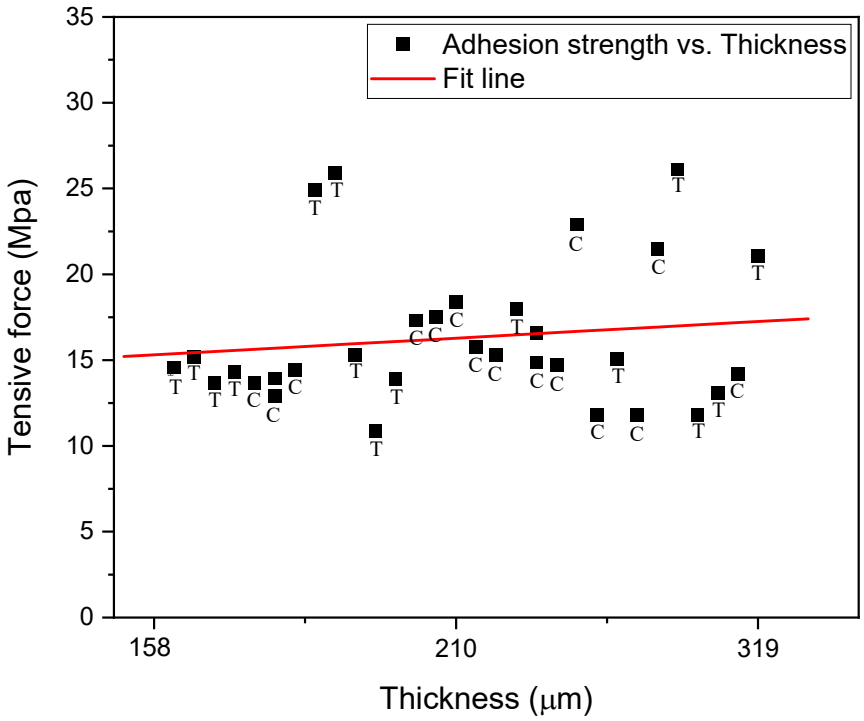

Figure 4. Pull-off adhesive strength as a function of the coating thickness for isothermal (C) and cycled (T) samples.

In conclusion, it was found that the adhesive strength increased after thermal exposure and the failure mode changed from failure mainly at the metal/adhesive interface to failure mainly within the coating, indicating that the interfacial bond strength between the substrate and coating improved after heating. The water-induced weakening of the adhesive could induce a reduction in adhesive energy at the metal interface [18]. After the coating was exposed to heat, the moisture content within the coating system decreases, thereby driving a shift in the dominant failure mode from adhesion to cohesion.

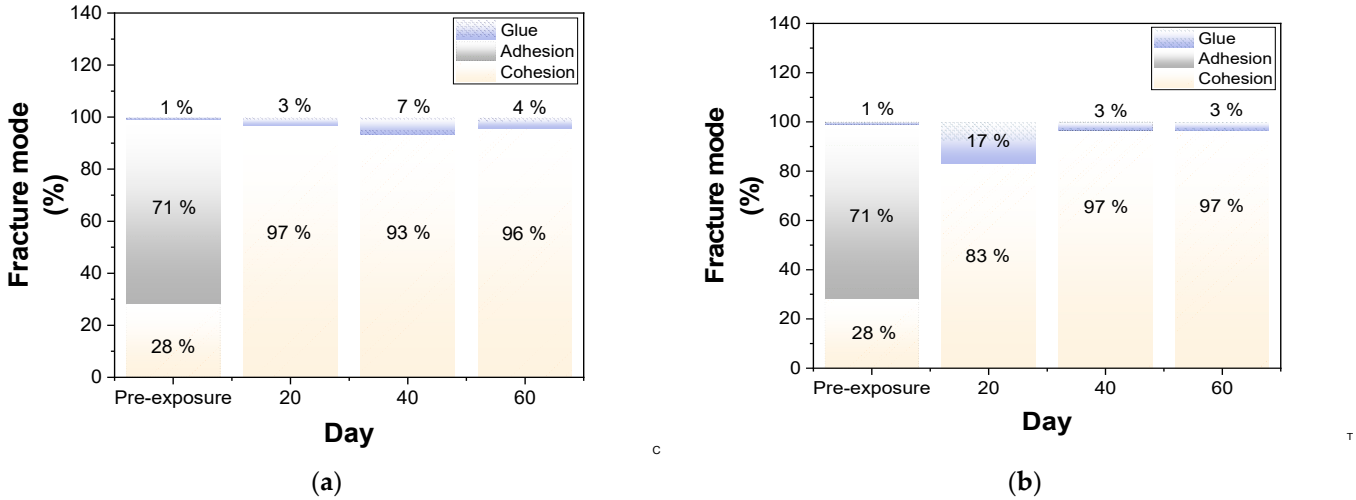

Figure 5. Area fractions of the failure modes of (**a**) isothermal and (**b**) cycled samples after pull-off adhesion tests.

3.2. Electrochemical Properties

The Nyquist plots of the electrochemical impedance of the coated panels show three distinct features, representing three different mechanisms (Figure 6). The pre-exposure sample showed low resistance. The EIS plots show semi-circles as capacitive loops that differ at high frequency and an oblique line at low frequency. These findings imply that a corrosive medium diffused into the coating–metal interface. The plot for the 120 °C isothermal sample is characterised by a single semi-circle with high impedance, suggesting that water penetrated the coating but did not reach the coating–metal interface. In contrast, the plot for the 150 °C isothermal sample shows double capacitive loops, indicating that the coating delaminated from the substrate (Figure 3).

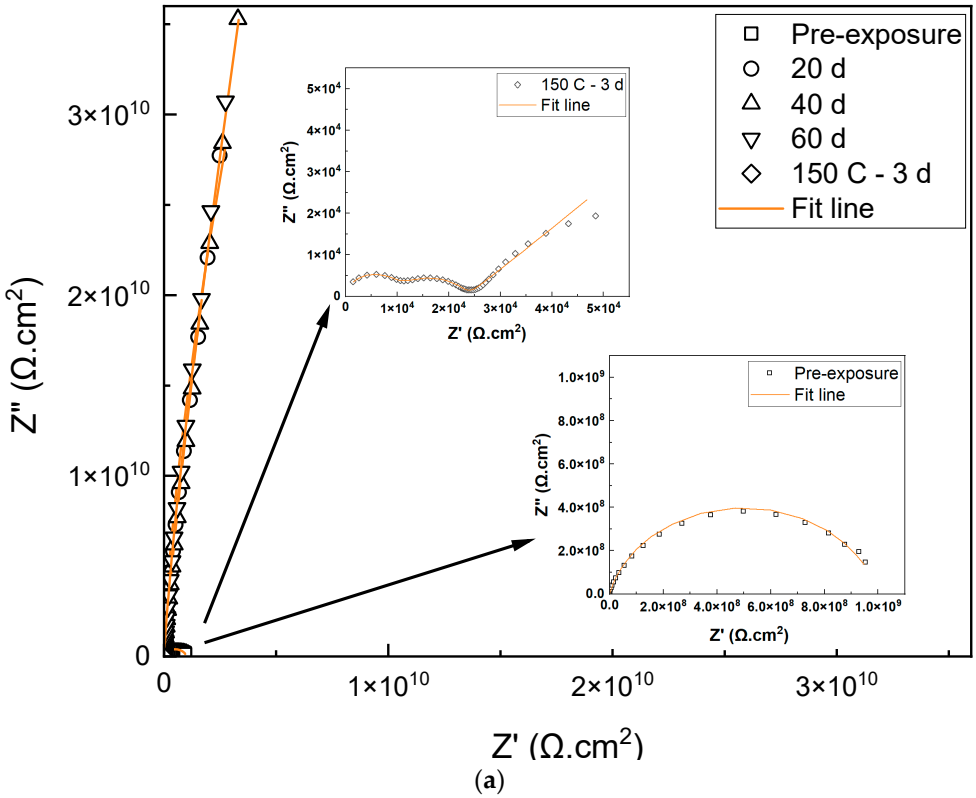

Figure 6. *Cont.*

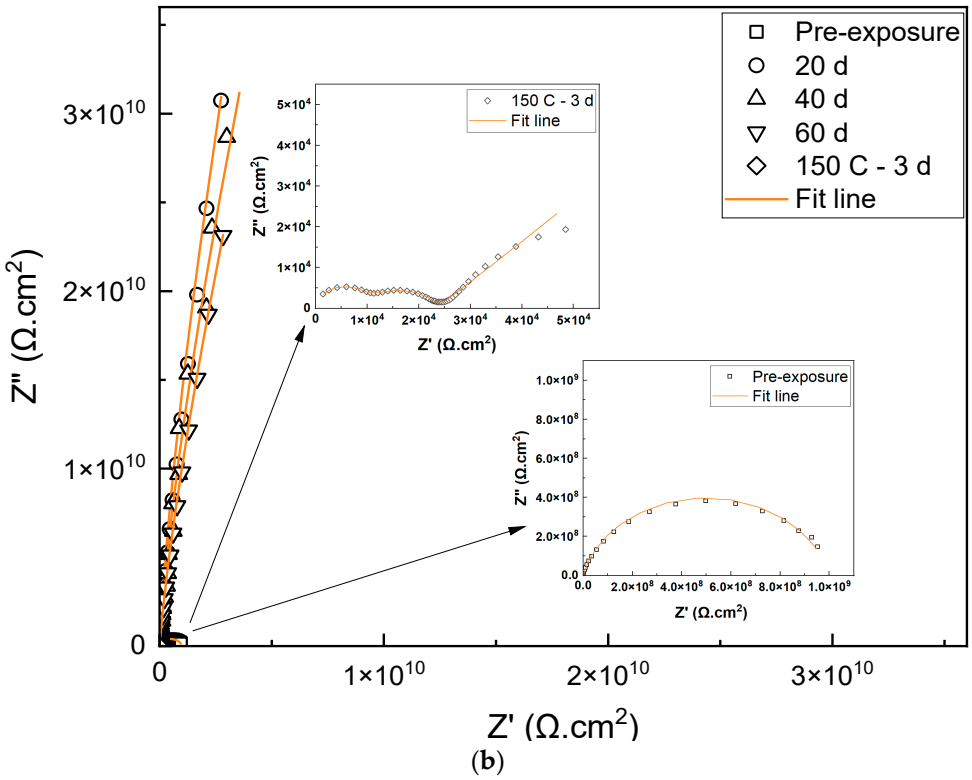

Figure 6. Nyquist plots of phenolic-epoxy-coated steel samples after immersion in 3.5 wt% NaCl solution: (**a**) cycled and (**b**) isothermal heat treatment (120 °C maximum temperature).

Figure 7 shows the evolution of Bode plots over time for the various thermal treatments. All coatings exhibited capacitive behaviour, with a single time constant covering a wide range of frequencies and a high impedance modulus at low frequency (indicating the resistance of the system) between 10^8 Ω·cm^2 for the pre-exposed samples and almost 10^{10} Ω·cm^2 for the coated samples after thermal treatment. The higher impedance of the coating after thermal treatment implies that exposing the coated panels to 120 °C forms a more durable barrier to the penetration of electrolytes. A simple equivalent circuit used for fitting the EIS data is shown in Figure 8a, comprising R_s, coating resistance R_{coat}, and CPE of the coating Q_{coat}. This circuit is commonly used for systems with a single time constant [19,20]. After 3 d of isothermal exposure to 150 °C, large cracks appeared on the coating (as shown in Figure 3), which may have resulted in the corrosion of the metal surface under the cracks due to electrolyte penetration before EIS was conducted. To account for the coating degradation, the EIS curves for this sample were fit using the modified equivalent electrical circuit presented in Figure 8b [21]. The shape of the plots for a coated metal, with two minima for the phase plot. The one at high frequency reflects the physical behaviour of the coating (Q_{coat}, R_{coat}), while the one at intermediate frequencies corresponds to the corrosion reactions at the coating–substrate interface (Q_{dl}, R_{ct}). The low R_{coat} and R_{ct} values indicate a low resistance to electrolyte diffusion through the coating and a significant corrosion reaction at the interface, respectively. The reactive impedance is equal to the sum of R_{ct} and R_s, i.e., 2.51 × 10^4 Ω·cm^2.

The data in Tables 3 and 4 summarise the resistance and capacitance values. The R_{coat} value increases from 10^8 Ω·cm^2 for the pre-exposure sample to 10^{10} Ω·cm^2 after thermal treatment. The maximum value of R_{coat} after 40 d of isothermal treatment was 3.18 × 10^{10} Ω·cm^2, while the highest equivalent value after thermal cycling was 3.38 × 10^{10} Ω·cm^2. Progressive improvement in the dielectric properties over time is also indicated by the Q_{coat} data. The Q_{coat} values for the coatings (10^{-10} F·cm^{-2}) exposed to isothermal treatment at 120 °C are much lower than that of the control (10^{-9} F·cm^{-2}). In addition, the Q_{coat} and Q_{dl} values for the coating exposed to isothermal heating at 150 °C

for 3 d increased compared to the control, implying the diffusion of corrosive species through the coating and contact with the metal substrate (Table 5).

Table 3. EIS fitting parameters for the 120 °C isothermal samples.

Duration (Days)	R_{coat} ($\Omega \cdot cm^2$)	Y_{coat} $S \cdot sec^n \cdot cm^{-2}$	n_{coat}	X^2
Pre-exposure	8.12×10^8	1.8×10^{-9}	0.84	5.55×10^{-3}
20 d	1.03×10^{10}	3.90×10^{-10}	0.965	8.05×10^{-4}
40 d	3.18×10^{10}	5.23×10^{-10}	0.994	3.63×10^{-3}
60 d	1.48×10^{10}	4.66×10^{-10}	0.977	1.46×10^{-4}

Table 4. EIS fitting parameters for the 120 °C cycled samples.

Duration (Days)	R_{coat} ($\Omega \cdot cm^2$)	Y_{coat} $S \cdot sec^n \cdot cm^{-2}$	n_{coat}	X^2
Pre-exposure	8.12×10^8	1.8×10^{-9}	0.84	5.55×10^{-3}
20 d	2.36×10^{10}	4.36×10^{-10}	0.991	1.46×10^{-4}
40 d	3.38×10^{10}	5.73×10^{-10}	0.998	9.48×10^{-4}
60 d	3.29×10^{10}	5.03×10^{-10}	0.968	1.51×10^{-4}

Table 5. EIS fitting parameters for the 150 °C isothermal samples after 3 d of exposure.

R_{coat} ($\Omega \cdot cm^2$)	R_{ct} ($\Omega \cdot cm^2$)	$Y_{coat}(S \cdot sec^n \cdot cm^{-2})$	n_{coat}	$Y_{dl}(S \cdot sec^n \cdot cm^{-2})$	n_{dl}	X^2
1.1×10^4	1.35×10^4	4.62×10^{-4}	0.98	2.14×10^{-7}	0.71	2.37×10^{-4}

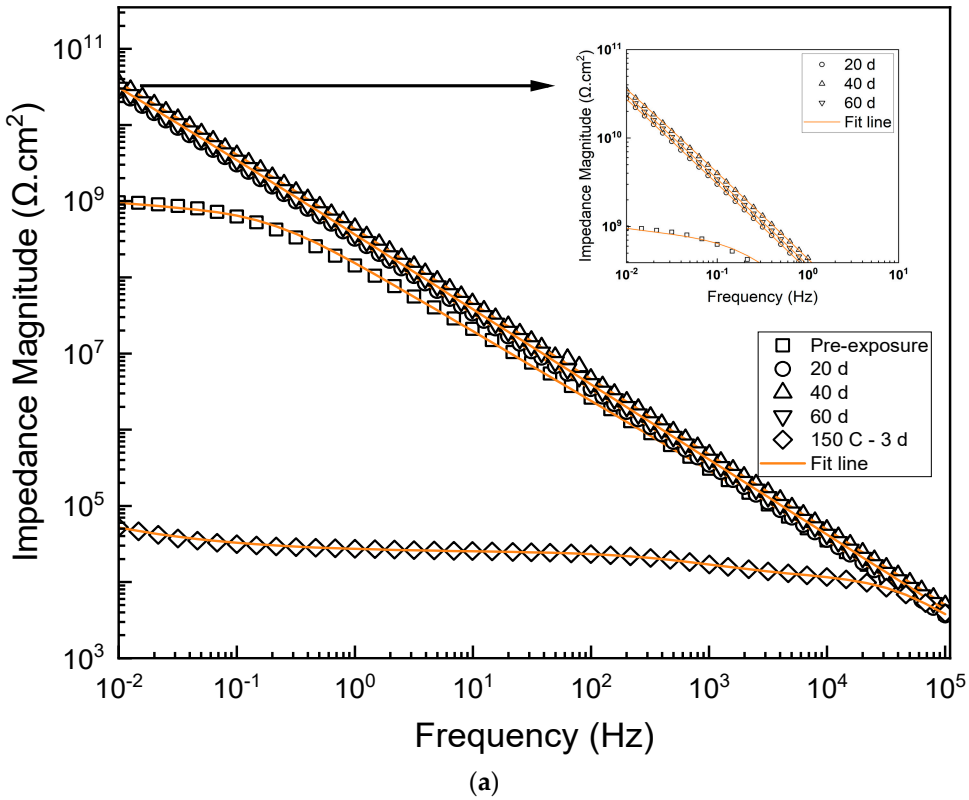

(**a**)

Figure 7. *Cont.*

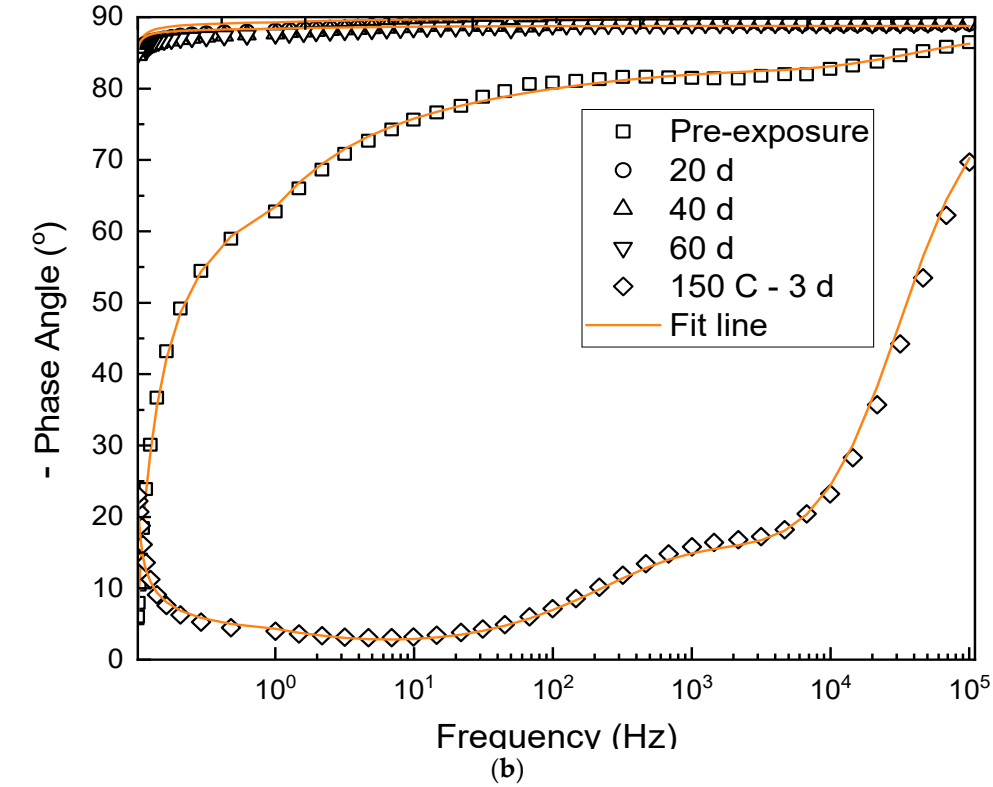

(**b**)

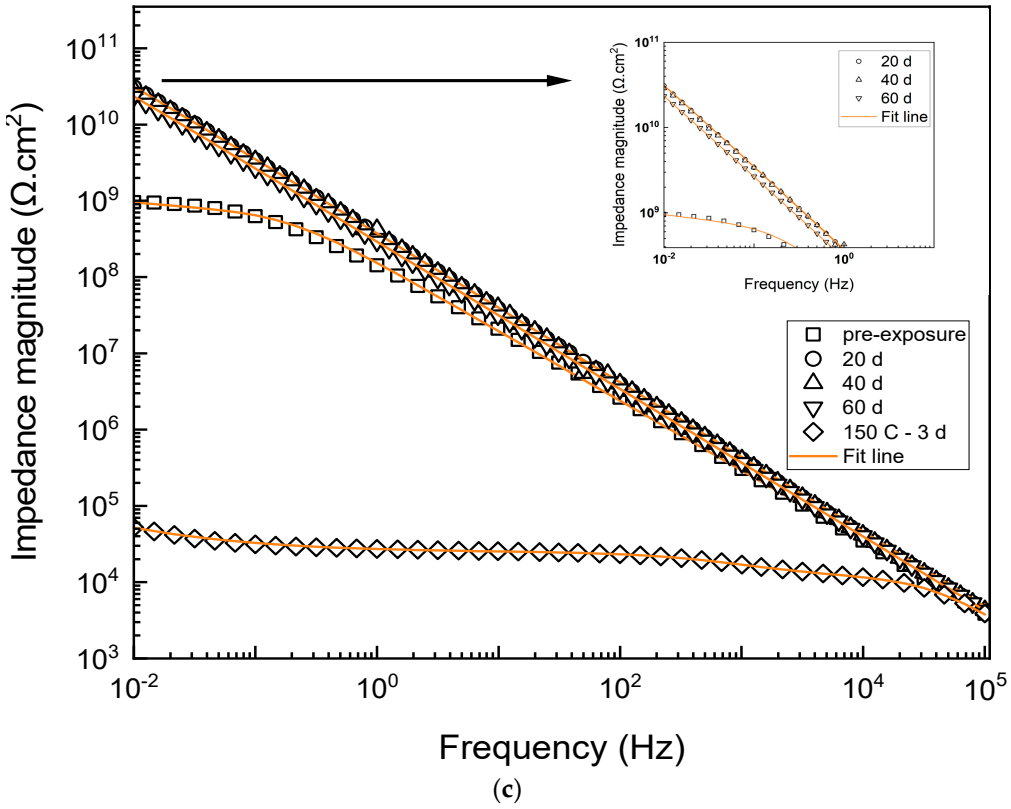

(**c**)

Figure 7. *Cont.*

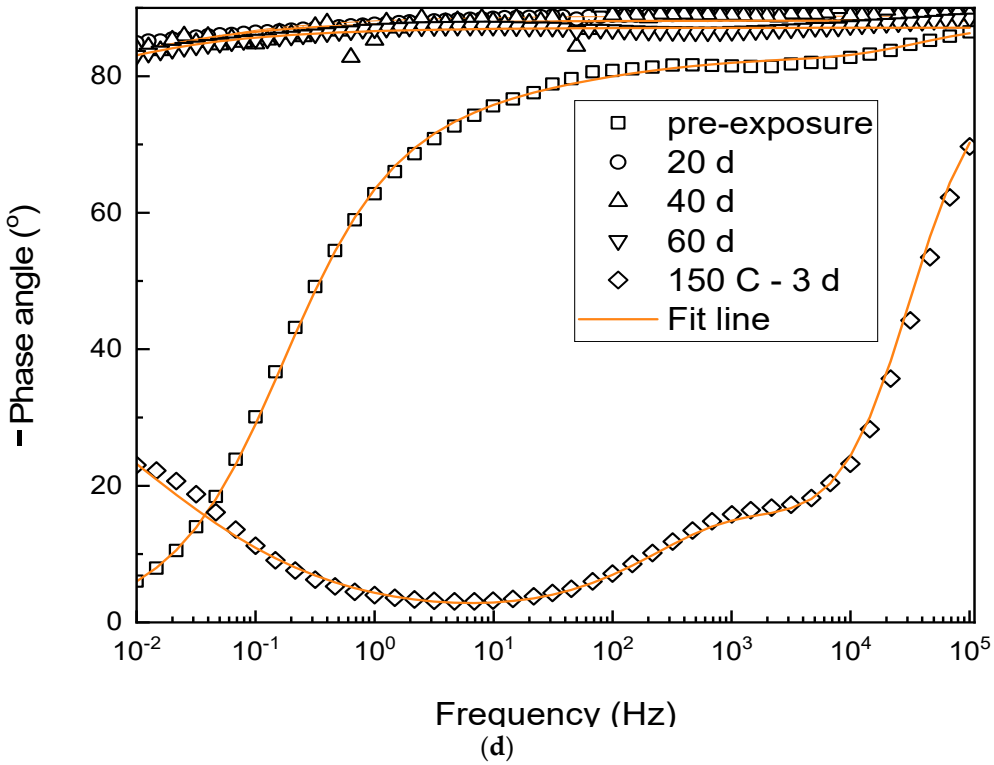

(**d**)

Figure 7. Bode plots of phenolic-epoxy-coated steel samples after immersion in 3.5 wt% NaCl solution: (**a**,**b**) cycled and (**c**,**d**) isothermal heat treatment (120 °C maximum temperature).

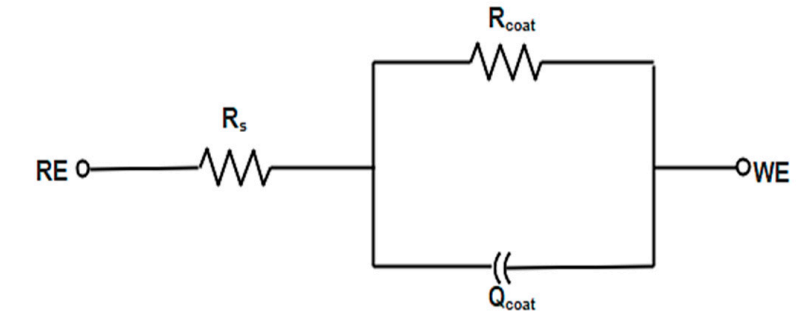

(**a**)

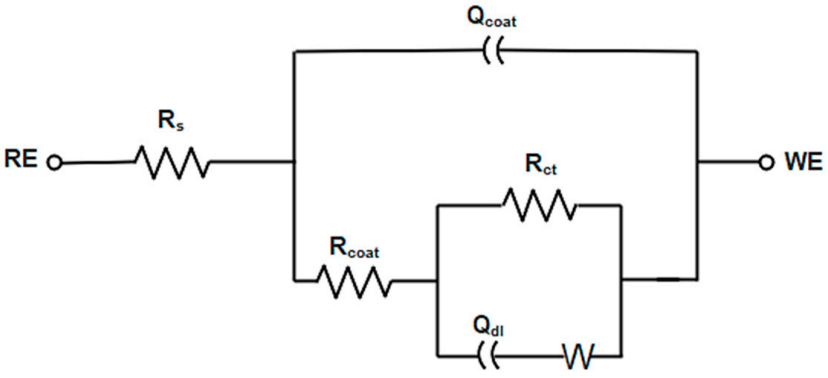

(**b**)

Figure 8. Equivalent circuits used to fit the impedance curves obtained for (**a**) all coated metal samples other than (**b**) the 150 °C isothermal sample (to account for cracks in the coating).

3.3. Thermal Behaviour

TGA and differential TGA (DTGA) results are shown in Figure 9. The major reactions are the dehydration of the coating with the formation of a double bond in the polymer chain, double bond isomerisation, and allyl-oxygen bond scission [22]. The DTGA curves in Figure 9b,d show a single endothermal peak at the same temperature region, close to 350 °C, for all coated panels. After heat treatment, two endothermic peaks are observed at 121 and 348 °C. This is due to the different temperature ranges of reactions of this sample. The peak at 121 °C could be due to the phase separation of the epoxy mixture during dehydration [23]. The second peak of the pre-exposure phenolic epoxy (at 348 °C) is considered the highest endothermic peak of all samples. This indicates that material decomposition accelerates at 348 °C [24]. Thermal damage during heating leads to a considerable loss of compounds, which in turn causes rapid degradation of the coating [23]. Subsequently, all coated panels show low endothermic peaks because of the formation of highly cross-linked structures and reduced reaction rates related to diminished chain mobility, which minimises the decomposition of compounds in the coating [23].

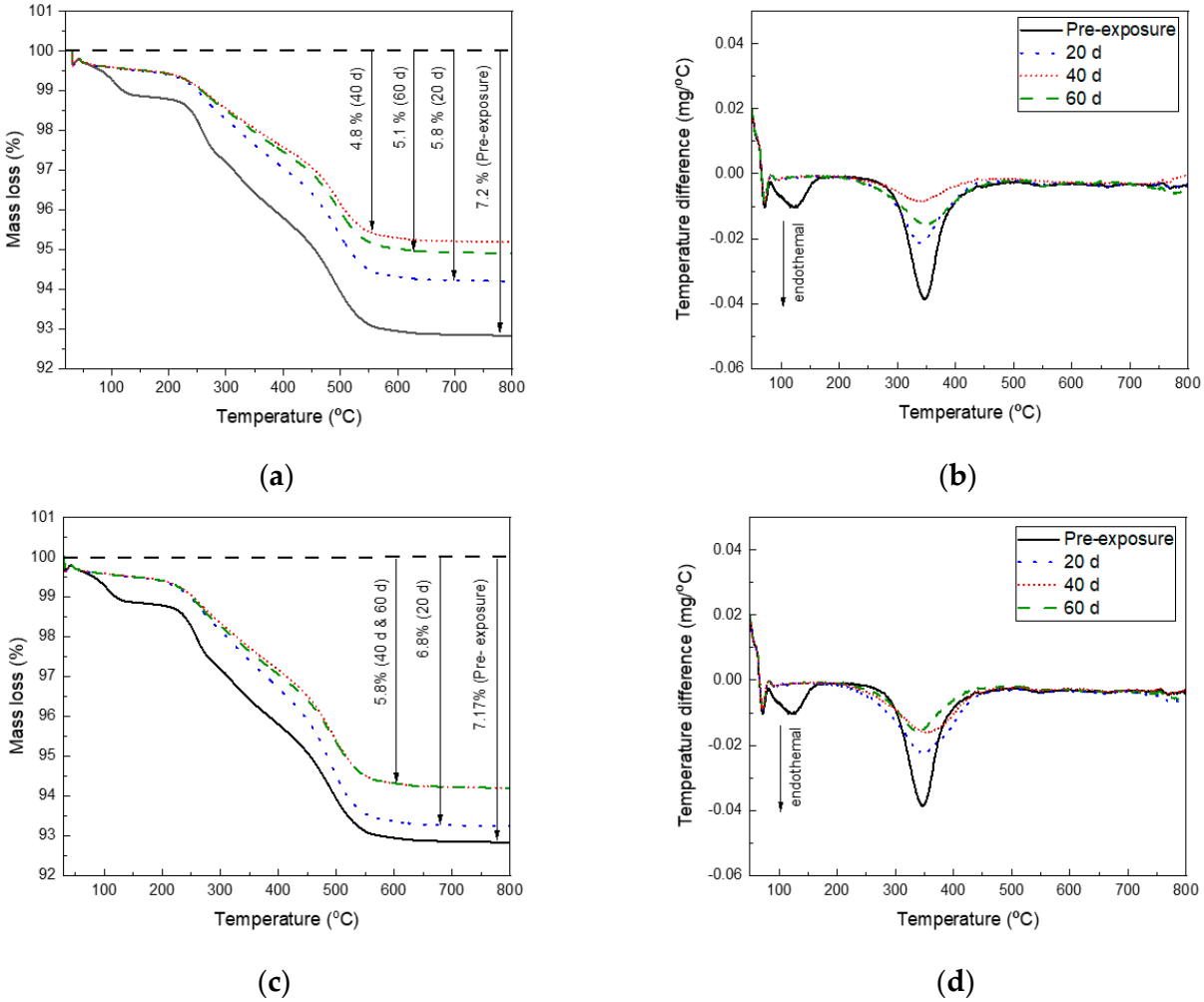

Figure 9. (**a**,**c**) TGA and (**b**,**d**) DTGA curves measured in air for phenolic-epoxy heat treated to a maximum of 120 °C under (**a**,**b**) isothermal or (**c**,**d**) cyclic conditions.

The T_g is an important parameter for identifying changes in the physical properties of polymers in their transition from a rigid glassy state to a softer rubbery state. The DSC curves used to determine the T_g values of the coated samples are shown in Figure 10. The lower T_g indicates the easier movement of molecules due to a less dense epoxy cross-linked network (lower MW) [25]. The T_g values of the phenolic-epoxy coating increased after

different periods of exposure to 120 °C. The initial T_g of 43.5 °C increased to 49.35 ± 1 °C after thermal cycling and 49.55 ± 1 °C after isothermal treatment for different durations. This emphasises that epoxy molecules have a high molecular chain strength and high MW after exposure to heating at 120 °C [25]. The pre-exposure coating shows two heat-flow peaks, corresponding to a melting process and the presence of organic solvents. Low-MW solvents have a large effect on the results of DSC purity determinations. The volatile impurities of substances with melting points above approximately 80 °C can evaporate [26].

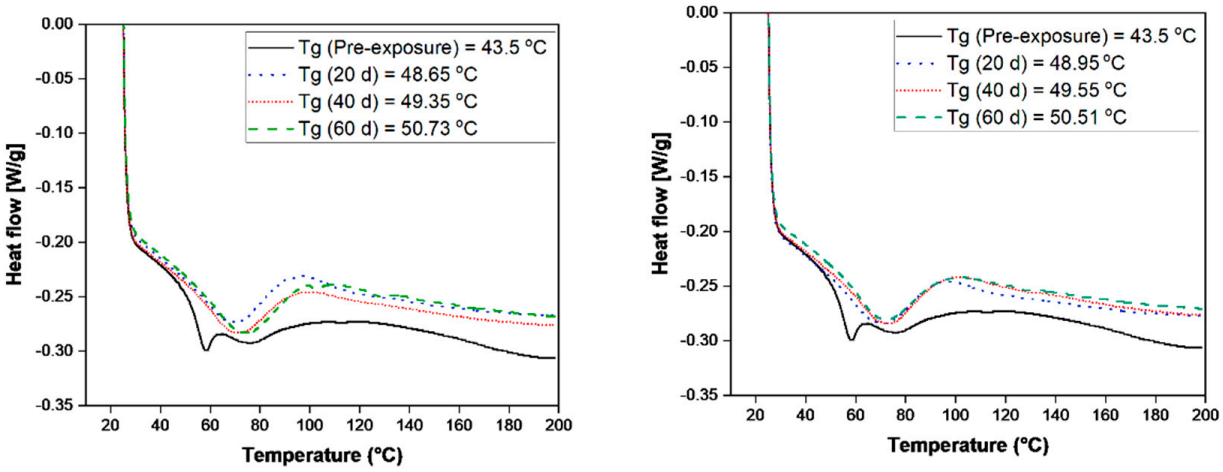

Figure 10. DSC curves used to determine the T_g values of phenolic epoxy coatings heat treated to a maximum of 120 °C under (**a**) isothermal or (**b**) cyclic conditions.

3.4. Chemical Properties

The FTIR spectra of the phenolic epoxy coatings exposed to different thermal conditions are shown in Figure 11. The absorption bands at 1650 and 1725 cm^{-1} increased with increasing exposure time, which could be due to the effect of the high temperature on the fresh coating, i.e., the formation of carbonyl groups [27]. In the hydroxyl domain (~3800–2500 cm^{-1}) [28], only minor changes were observed after 40 d of heat treatment. The C=C stretching vibration is normally observed at 1665–1675 cm^{-1} for the trans configuration and at 1635–1665 cm^{-1} for the cis configuration [28]. Consequently, the prominent band at 1730 cm^{-1} is assigned to the characteristic C=O stretching frequency [29].

The molecular-level changes in the structure that can occur in the phenolic epoxy-coating during thermal treatment are illustrated below. A representative molecular structure of epoxy resins (diglycidyl ether of bisphenol A; DGEBA) is shown in Figure 12. To interpret the thermal behaviour of the epoxy resin, the simplest DGEBA resin with $n = 0$ is considered. Moreover, the curing of epoxy resin systems is strongly dependent on the type of hardener. To explain the structure of the heat-treated resins as simply as possible, an aliphatic amine curing agent, ethylene diamine (EDA), is considered. A stoichiometric mixture contains two molecules of EDA bonded with two molecules of DGEBA. The structure of the resultant product is shown in Figure 13a. The carbonyl group formed in an epoxy resin is surrounded by adjacent –CH_2–groups. The bands at 1725 cm^{-1} are assigned to the characteristic C=O stretch frequency, which is expected to result in absorption in the region for alkyl-substituted carbonyls [27]. The presence of double bonds in the amine linkages is indicated by the C=C stretching vibration. These peaks at 1650 cm^{-1} are the result of shifting alkane frequencies arising from adjacent amine groups [28]. The changes in the structure of the carbonyl groups form pendant –OH groups, and double bonds form in the amine linkages of the epoxy resin. Reactions involving the evolved hydrogen, such as the formation of carbonyl groups and double bonds in the amine linkage, and possibly cross-linking between molecules, are shown in Figure 13b. These reactions tend to make

the molecular network more rigid, thus affecting the mechanical properties, as shown in Table 2 and Figure 5.

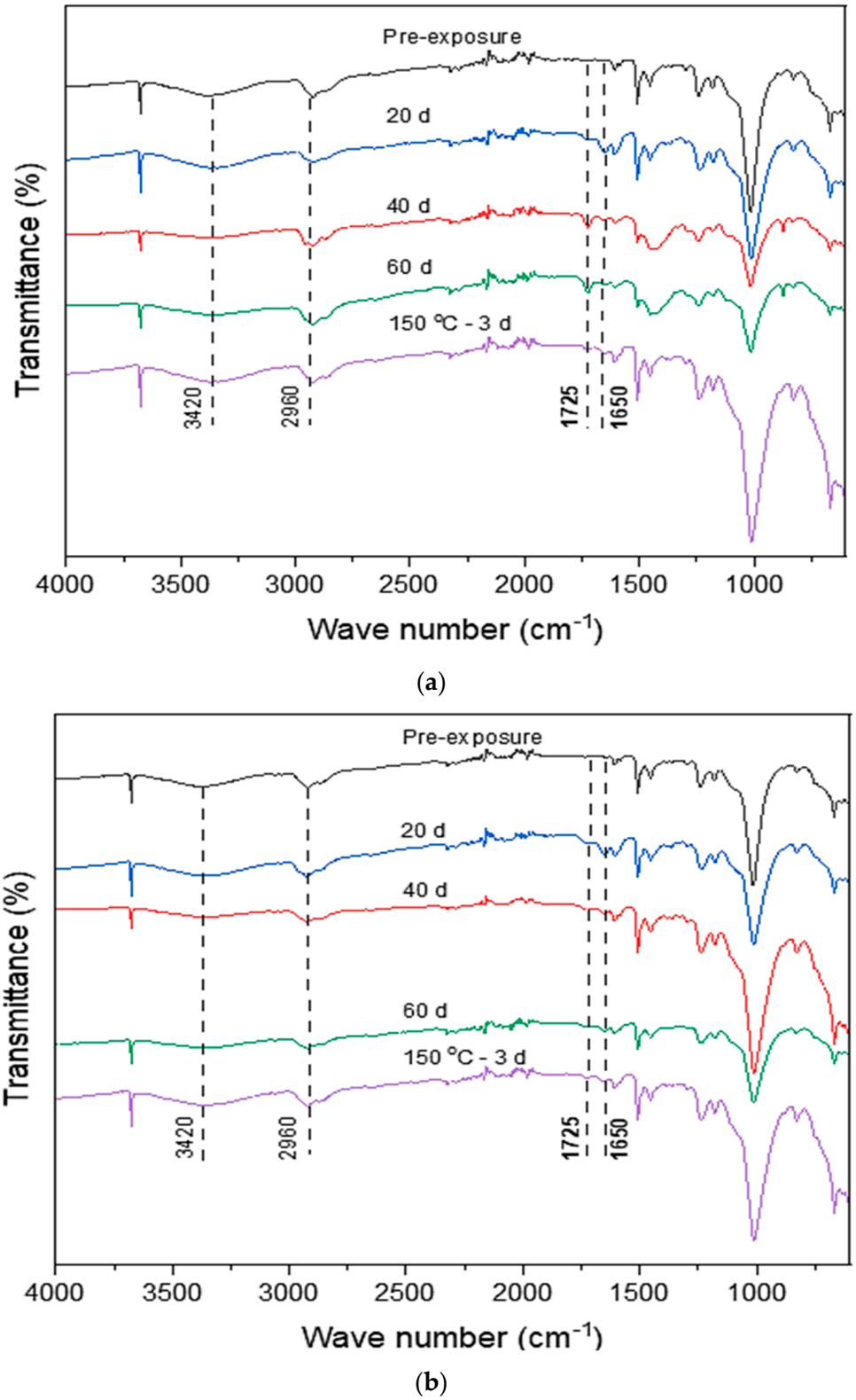

Figure 11. FTIR spectra phenolic epoxy coatings before and after heat treatment to a maximum of 120 °C under (**a**) cyclic or (**b**) isothermal.

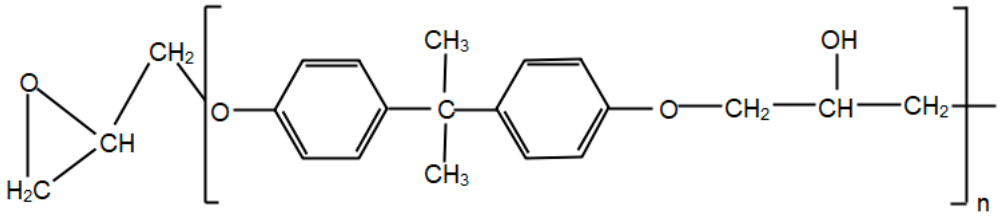

Figure 12. Chemical structure of DGEBA as a typical resin.

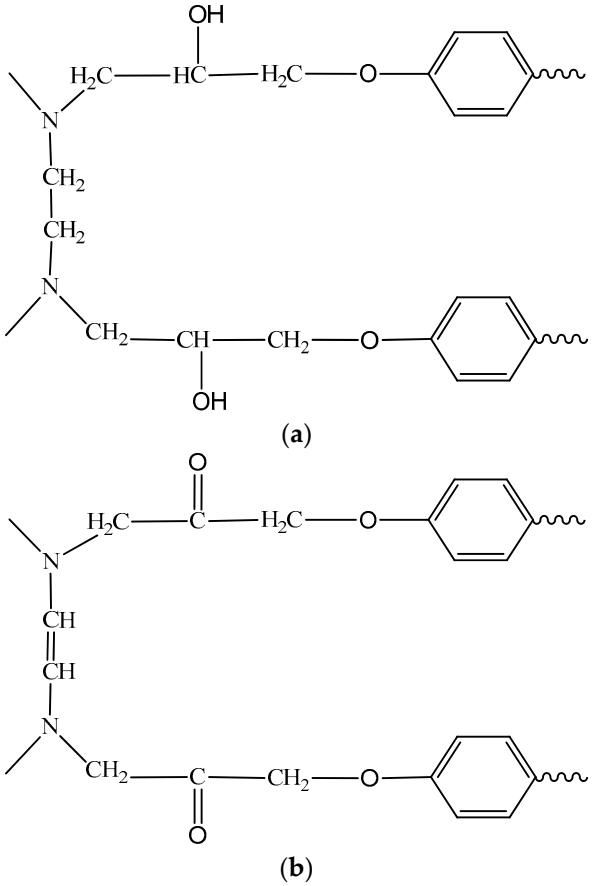

Figure 13. Chemical structures produced during the resin curing reaction between DGEBA and EDA hardener (**a**) before and (**b**) after heat exposure [28].

3.5. Molecular Structure of the Coatings

The molecular composition of the coatings was studied by ToF-SIMS. Figure 14 shows a variation in the intensity of the secondary ion peaks of positive ions for the coatings used in this study (exposed to three different thermal treatment conditions). The assignments of the peaks were initially based on reference libraries and the literature for DGEBA [28–31]. The $C_xH_yO^+$ ions were identified as the single-ring ions in the resin, while the nitrogen-containing hydrocarbon ions ($C_xH_yN^+$) are related to the epoxy hardener, and the aliphatic hydrocarbon ions (C_xH^+) indicate structural density [30]. The MW of the hydrocarbon ions provides significant information about the cross-linking to the hydrocarbon structure in the phenolic epoxy coatings. The ToF-SIMS analysis focused on the sample with the highest adhesion strength, which was subjected to thermal cycling between 22 °C and 120 °C for 40 d. Cracks were present on the coating of the similar sample cycled to 150 °C. To investigate the differences between these samples, ToF-SIMS was used to investigate the molecular composition of the coating to identify the changes in the epoxy structure at high temperatures.

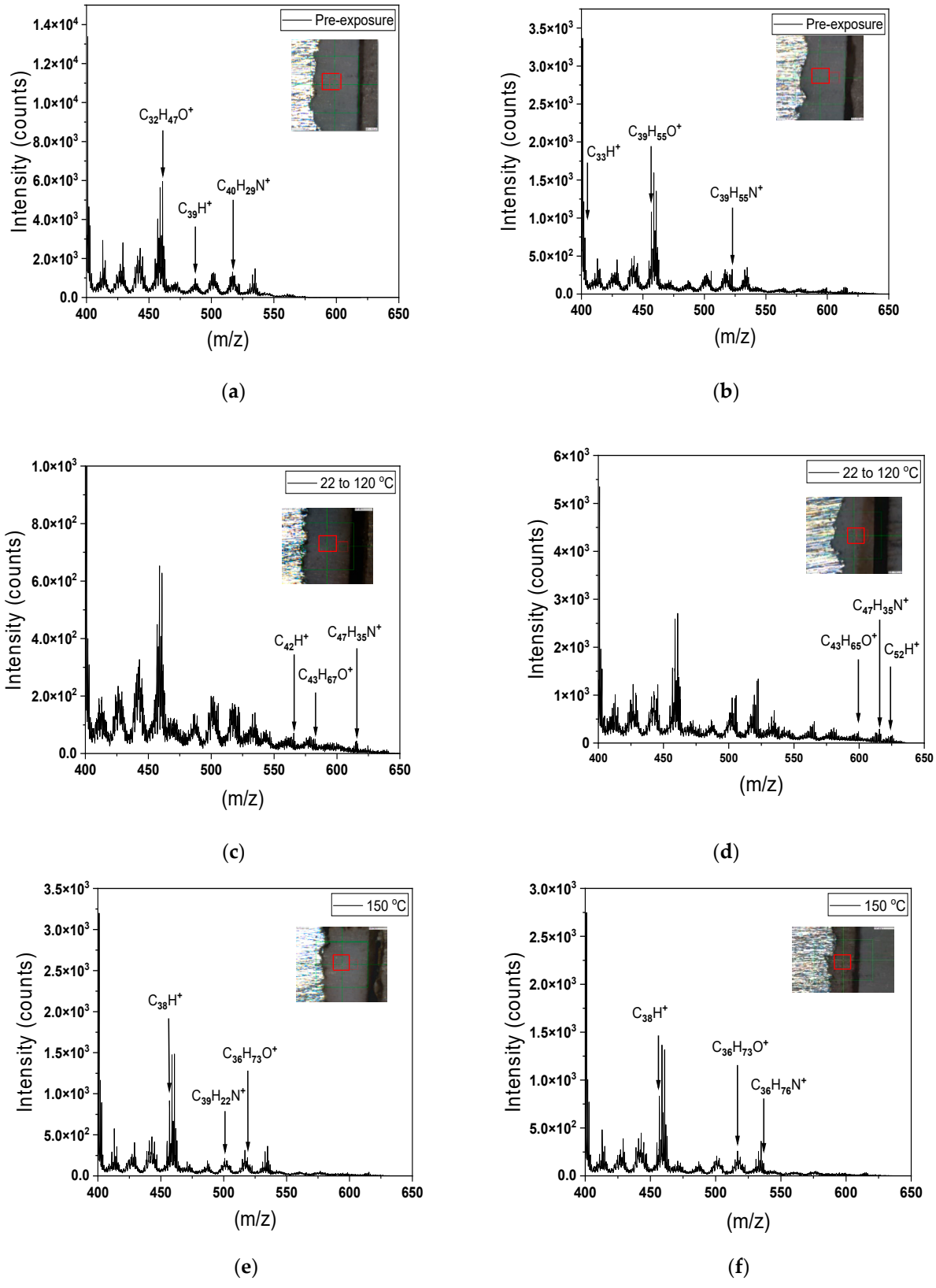

Figure 14. Positive ion ToF-SIMS spectra (field of view 0.1 mm × 0.1 mm, indicated in the inset optical microscopy images of cross-sections of single-layer coatings). The highest MW ions ($CxHyO^+$, $CxHyN^+$, and CxH^+) with intensities above 10 counts are labelled. (**a**,**b**) Pre-exposure, (**c**,**d**) cyclic treatment up to 120 °C for 40 d, and (**e**,**f**) isothermal treatment at 150 °C for 3 d. The red boxes are ToF-SIMS scan locations on a coating film.

Measurements were taken at two locations for each coating, as indicated by the red squares in the inset microscopy images in Figure 14. The mass range of 400–640 m/z shows contributions from three high-MW components. The highest aliphatic hydrocarbon weight was identified for $C_{33}H^+$, $C_{39}H^+$, $C_{42}H^+$, $C_{52}H^+$, and $C_{38}H^+$ for all three thermal conditions. The results for the unexposed control sample were compared with those for the heat-treated samples (thermal cycling to 120 °C or isothermal treatment at 150 °C). The cycled sample had the highest MW and the aliphatic hydrocarbon was $C_{52}H^+$, which indicates enhanced cross-linking between the epoxy resin and curing agent (hardener) during thermal exposure [31]. At the higher temperature of 150 °C, epoxy chain scission occurred, resulting in a reduction in C–C bonding. A reduction in aliphatic hydrocarbon indicates a network rupture and a reduction in network density, which is due to the low MW aliphatic hydrocarbon $C_{38}H^+$. Other explanations might be a heat-induced condensation reaction or the formation of polyaromatic structures at the surface [30,31].

The other significant polymer group is resin molecules, which is indicated by the oxygen-containing hydrocarbon molecules revealed by the ToF-SIMS positive ion spectra (Figure 14). $C_{32}H_{47}O^+$, $C_{39}H_{55}O^+$, $C_{43}H_{67}O^+$, $C_{43}H_{65}O^+$, $C_{32}H_{60}O^+$, and $C_{36}H_{73}O^+$ were observed for the resin material. No differences attributable to the network density were observed in the spectra of the sample treated at 150 °C and the unexposed control sample. The increased development of hydrocarbon molecules during thermal cycling increased the MW of the resin material to $C_{43}H_{67}O^+$. This indicates that the cross-linking of the resin enhanced the oligomer bonds and distributions in the resin. This chain length provides better-balanced mechanical and thermal properties [28].

Another contribution appears in the $C_xH_yN^+$ ion fragments, such as $C_{40}H_{29}N^+$, $C_{39}H_{29}N^+$, $C_{47}H_{35}N^+$, $C_{39}H_{22}N^+$, and $C_{36}H_{76}N^+$. Figure 14 show significant changes in long-chain hydrocarbon ions that contain nitrogen. The structural density and cross-linking reactions in the hardener component increased when the coating was exposed to thermal cycling for 40 days, reaching $C_{47}H_{35}N^+$. This indicates a discrete physical phenomenon in which the concentrations of ions produced during thermal cycling increase in the hardener and resin. The structural changes at the interfaces of adhesive joints provide valuable information regarding the adhesive/coating surface and interfaces (adhesion chemistry).

In the case of the sample treated at 150 °C, the hydrocarbon ions containing nitrogen ($C_{40}H_{29}N^+$ to $C_{36}H_{76}N^+$) had lower MW than those identified for the control sample. The hardener component suffered chain scission as a result of thermomechanical stresses, resulting in structural damage [31]. Thermal stress generates mechanical pressure at the surface and in the bulk resulting in crack initiation and propagation. Organics coatings can be damaged at elevated temperatures due to the outgassing of volatiles, dehydration, and shrinkage, where the latter results in the generation of cracks [29].

The ToF-SIMS results provide information about structural changes at the interfaces in adhesive joints, in addition to the interfacial chemistry of the adhesive/coating surface. The results indicated that the molecular composition of the sample changed after heating, observed as changes in the intensities of ions reported to be related to the chain structure of epoxy components, which are consistent with the mechanical testing results.

4. Conclusions

This study investigated the chemical and physical changes of phenolic–epoxy coatings after exposure to elevated temperatures. The following conclusions were drawn:

- Phenolic-epoxy coatings underwent post-curing when exposed to 120 °C for up to 40 d, resulting in enhanced coating performance, as demonstrated by the increased adhesion strengths and high impedance of the coatings.
- After further exposure for 60 d, the opposite results were obtained; i.e., coating degradation was evidenced by lower adhesion strengths.
- The ToF-SIMS results demonstrated enhanced cross-linking after thermal exposure due to the generation of larger hydrocarbon fragments.

- In contrast, increasing the dry temperature from 120 to 150 °C led to a loss of hydrocarbon weight, resulting in cracking of the coating surface.
- Optimised dry-film thickness of phenolic-epoxy coating after heat treatment to provide maximum substrate protection.

Author Contributions: Conceptualization, S.A., T.P., X.S., W.D.A.R. and K.L.; methodology, S.A., T.P., X.S. and W.D.A.R.; validation, T.P., X.S. and W.D.A.R.; formal analysis, T.P., X.S. and W.D.A.R.; investigation, T.P.; data curation, T.P., X.S. and W.D.A.R.; writing–original draft preparation, S.A., T.P. and W.D.A.R.; writing–review and editing, T.P.; visualization, T.P.; supervision, T.P. and K.L.; project administration, T.P.; funding acquisition, T.P. All authors have read and agreed to the published version of the manuscript.

Funding: This research received no external funding.

Data Availability Statement: The data presented in this study are available on request from the corresponding author.

Acknowledgments: We would like to express our appreciation for the support provided by the Curtin Corrosion Centre and WA School of Mines: Minerals, Energy and Chemical Engineering at Curtin University. We would also like to acknowledge the sponsorship that we received from Royal Saudi Naval Forces. Finally, we thank the Microscopy and Microanalysis Facilities at Curtin University for allowing us to conduct ToF-SIMS at their facility.

Conflicts of Interest: The authors declare no conflict of interest.

References

1. Bierwagen, G.P. Reflections on corrosion control by organic coatings. *Prog. Org. Coat.* **1996**, *28*, 43–48. [CrossRef]
2. Croll, S.G. Stress and embrittlement in organic coatings during general weathering exposure: A review. *Prog. Org. Coat.* **2022**, *172*, 107085. [CrossRef]
3. Tennent, N.H. Clear and pigmented epoxy resins for stained glass conservation: Light ageing studies. *Stud. Conserv.* **1979**, *24*, 153–164. [CrossRef]
4. Fast, D.; A Two Step Solution to the High Cost of Corrosion under Insulation. Corrosionpedia 2020, p. 7. Available online: https://www.corrosionpedia.com/2/6495/corrosion-under-insulation-cui/a-two-step-solution-to-the-high-cost-of-corrosion-under-insulation (accessed on 25 February 2024).
5. Dagdag, O.; Hsissou, R.; Berisha, A.; Erramli, H.; Hamed, O.; Jodeh, S.; El Harfi, A. Polymeric-Based Epoxy Cured with a Polyaminoamide as an Anticorrosive Coating for Aluminum 2024-T3 Surface: Experimental Studies Supported by Computational Modeling. *J. Bio-Tribo-Corros.* **2019**, *5*, 58. [CrossRef]
6. Bahlakeh, G.; Ghaffari, M.; Saeb, M.R.; Ramezanzadeh, B.; De Proft, F.; Terryn, H. A Close-up of the Effect of Iron Oxide Type on the Interfacial Interaction between Epoxy and Carbon Steel: Combined Molecular Dynamics Simulations and Quantum Mechanics. *J. Phys. Chem. C* **2016**, *120*, 11014–11026. [CrossRef]
7. Hsissou, R.; El Harfi, A. Application of pentaglycidyl ether penta-ethoxy phosphorus composites polymers formulated by two additives, trisodium phosphate (TSP) and natural phosphate(NP) and their combination in the behavior of the coating on E24 carbon steel in NaCl 3.5%. *Anal. Bioanal. Electrochem.* **2018**, *10*, 728–738.
8. Hsissou, R.; Dagdag, O.; Berradi, M.; El Bouchti, M.; Assouag, M.; Elharfi, A. Development rheological and anti-corrosion property of epoxy polymer and its composite. *Heliyon* **2019**, *5*, e02789. [CrossRef]
9. Hsissou, R.; Dagdag, O.; Abbout, S.; Benhiba, F.; Berradi, M.; El Bouchti, M.; Berisha, A.; Hajjaji, N.; Elharfi, A. Novel derivative epoxy resin TGETET as a corrosion inhibition of E24 carbon steel in 1.0 M HCl solution. Experimental and computational (DFT and MD simulations) methods. *J. Mol. Liq.* **2019**, *284*, 182–192. [CrossRef]
10. Es-Sahbany, H.; Berradi, M.; Nkhili, S.; Hsissou, R.; Allaoui, M.; Loutfi, M.; Bassir, D.; Belfaquir, M.; El Youbi, M.S. Removal of heavy metals (nickel) contained in wastewater-models by the adsorption technique on natural clay. *Mater. Today Proc.* **2019**, *13*, 866–875. [CrossRef]
11. Ogata, M.; Kinjo, N.; Kawata, T. Effects of crosslinking on physical properties of phenol–formaldehyde novolac cured epoxy resins. *J. Appl. Polym. Sci.* **1993**, *48*, 583–601. [CrossRef]
12. Charlesworth, J.M. Effect of crosslink density on the molecular relaxations in diepoxide-diamine network polymers. Part 1. The glassy region. *Polym. Eng. Sci.* **1988**, *28*, 221–229. [CrossRef]
13. *ISO 19277:2018*; Petroleum, Petrochemical and Natural Gas. International Organization for Standardization: Geneva, Switzerland, 2018; Volume 2012, p. 12.
14. *ASTM D4541-09*; Standard Test Method for Pull-Off Strength of Coatings Using Portable Adhesion. ASTM International: West Conshohocken, PA, USA, 2014. [CrossRef]

15. Prime, R.B.; Bair, H.E.; Vyazovkin, S.; Gallagher, P.K.; Riga, A. Thermogravimetric Analysis (TGA). In *Thermal Analysis of Polymers: Fundamentals and Applications*; Wiley and Sons Inc.: Hoboken, NJ, USA, 2008; ISBN 9780471769170.
16. Singh, R.; Schruefer, S.; Wilson, S.; Gibmeier, J.; Vassen, R. Influence of coating thickness on residual stress and adhesion-strength of cold-sprayed Inconel 718 coatings. *Surf. Coat. Technol.* **2018**, *350*, 64–73. [CrossRef]
17. Kambhampati, S.; Pojtanabuntoeng, T. A systemic study on the effects of key influencing factors on pull-off adhesion test of organic coatings. *Corros. Sci. Eng.* **2023**, *1*, 11.
18. Li, X.; Deng, S.; Fu, H. Blue tetrazolium as a novel corrosion inhibitor for cold rolled steel in hydrochloric acid solution. *Corros. Sci.* **2010**, *52*, 2786–2792. [CrossRef]
19. Mahdavian, M.; Ashhari, S. Mercapto functional azole compounds as organic corrosion inhibitors in a polyester-melamine coating. *Prog. Org. Coat.* **2010**, *68*, 259–264. [CrossRef]
20. Granata, R.D. *Polymer Coating Degradation Mechanisms Related to Hot Production*; Defense Technical Information Center: Houston, TX, USA, 1993.
21. Morancho, J.M.; Salla, J.M.; Ramis, X.; Cadenato, A. Comparative study of the degradation kinetics of three powder thermoset coatings. *Thermochim. Acta* **2004**, *419*, 181–187. [CrossRef]
22. Puglia, D.; Manfredi, L.B.; Vazquez, A.; Kenny, J.M. Thermal degradation and fire resistance of epoxy-amine-phenolic blends. *Polym. Degrad. Stab.* **2001**, *73*, 521–527. [CrossRef]
23. Kandola, B.K.; Biswas, B.; Price, D.; Horrocks, A.R. Studies on the effect of different levels of toughener and flame retardants on thermal stability of epoxy resin. *Polym. Degrad. Stab.* **2010**, *95*, 144–152. [CrossRef]
24. Sarathi, R.; Sahu, R.K.; Rajeshkumar, P. Understanding the thermal, mechanical and electrical properties of epoxy nanocomposites. *Mater. Sci. Eng. A* **2007**, *445*, 567–578. [CrossRef]
25. Zaccone, A.; Terentjev, E.M. Disorder-assisted melting and the glass transition in amorphous solids. *Phys. Rev. Lett.* **2013**, *110*, 178002. [CrossRef]
26. van Dooren, A.A.; Müller, B.W. Purity determinations of drugs with differential scanning calorimetry (DSC)-a critical review. *Int. J. Pharm.* **1984**, *20*, 217–233. [CrossRef]
27. Alpert, N.L.; Keiser, W.E.; Szymanski, H.A. IR—Theory and practice of infrared spectroscopy. *J. Mol. Struct.* **1974**, *23*, 320. [CrossRef]
28. Treverton, J.A.; Paul, A.J.; Vickerman, J.C. Characterization of adhesive and coating constituents by time-of-flight secondary ion mass spectrometry (ToF-SIMS). Part 1: Epoxy-terminated diglycidyl polyethers of bisphenol-A and propal-2-ol. *Surf. Interface Anal.* **1993**, *20*, 449–456. [CrossRef]
29. Decelle, J.; Huet, N.; Bellenger, V. Oxidation induced shrinkage for thermally aged epoxy networks. *Polym. Degrad. Stab.* **2003**, *81*, 239–248. [CrossRef]
30. Awaja, F.; Van Riessen, G.; Kelly, G.; Fox, B.; Pigram, P.J. Tof-sims investigation of epoxy resin curing reaction at different resin to hardener ratios. *J. Appl. Polym. Sci.* **2008**, *110*, 2711–2717. [CrossRef]
31. Awaja, F.; Pigram, P.J. Surface molecular characterisation of different epoxy resin composites subjected to UV accelerated degradation using XPS and ToF-SIMS. *Polym. Degrad. Stab.* **2009**, *94*, 651–658. [CrossRef]